The Influence of Nonlinear Mesoscale Eddies on Near-Surface Oceanic Chlorophyll

Dudley B. Chelton *et al.*

Science **334**, 328 (2011);
DOI: 10.1126/science.1208897

Science (print ISSN 0036-8075; online ISSN 1095-9203) is published weekly, except the last week in December, by the American Association for the Advancement of Science, 1200 New York Avenue NW, Washington, DC 20005.

The Influence of Nonlinear Mesoscale Eddies on Near-Surface Oceanic Chlorophyll

Dudley B. Chelton,[1]* Peter Gaube,[1] Michael G. Schlax,[1]
Jeffrey J. Early,[2] Roger M. Samelson[1]

Oceanic Rossby waves have been widely invoked as a mechanism for large-scale variability of chlorophyll (CHL) observed from satellites. High-resolution satellite altimeter measurements have recently revealed that sea-surface height (SSH) features previously interpreted as linear Rossby waves are nonlinear mesoscale coherent structures (referred to here as eddies). We analyze 10 years of measurements of these SSH fields and concurrent satellite measurements of upper-ocean CHL to show that these eddies exert a strong influence on the CHL field, thus requiring reassessment of the mechanism for the observed covariability of SSH and CHL. On time scales longer than 2 to 3 weeks, the dominant mechanism is shown to be eddy-induced horizontal advection of CHL by the rotational velocities of the eddies.

A decade of concurrent satellite measurements of sea surface height (SSH) and upper-ocean chlorophyll (CHL) is enabling studies of physical-biological interaction that are not feasible from ship-based observations. Although satellites provide only near-surface information about ocean physics and biology, they are the only practical means of obtaining dense, global observations. Altimetric measurements of SSH reveal that westward propagation is ubiquitous (*1*) with characteristics similar to the linear Rossby waves by which the ocean adjusts to wind and thermal forcing (*2*). Westward propagation is also evident in CHL estimates derived from satellite measurements of ocean color. The widespread interpretation of the westward-propagating SSH variations as Rossby waves led naturally to interpretations that the CHL variations are also induced by Rossby waves (*3*–*5*).

The mechanism for Rossby wave influence on CHL has been debated (*4*–*9*), in part because of inconsistency in the lag between variations of SSH and CHL. The most widely accepted view is that the covariability between SSH and CHL arises from cyclical advection of CHL by the horizontal velocity field associated with passing Rossby waves (*7*–*9*).

The prevailing view before the recent focus on Rossby wave influence was that CHL concentration is influenced by nonlinear eddies (*10*–*15*). Investigations of this eddy influence have continued in parallel with Rossby wave studies. Here, we show that the copropagation of CHL and SSH previously interpreted as having been caused by Rossby waves is in fact attributable to eddies.

Nonlinearity of SSH variability. High-resolution SSH fields produced by merging the measurements from two simultaneously operating satellite altimeters (*16*) reveal that westward-propagating features previously believed to be linear Rossby waves are actually nonlinear rotating coherent structures ("eddies") with radii of ~100 km (*17*, *18*). Because such mesoscale features propagate westward with approximately the speed of long Rossby waves (*17*–*19*), they can masquerade as Rossby waves in low-resolution SSH fields constructed from measurements by a single altimeter.

The degree of nonlinearity of a mesoscale feature is characterized by the ratio of the rotational fluid speed U to the translation speed c of the feature. When $U/c > 1$, the feature is nonlinear, which allows it to maintain a coherent structure as it propagates (*20*). This requires that all of the wavelength components of the feature propagate at the same speed, i.e., nondispersively. With linear Rossby wave dynamics, features that are initially spatially compact quickly lose their coherent structure through dispersion (*21*).

At latitudes higher than 25°, 98% of the features tracked for ≥10 weeks have $U/c > 1$ (fig. S2). The degree of nonlinearity is slightly less at lower latitudes where the propagation speeds c are faster (*17*, *18*). But even in the latitude range 15° to 25°, 95% of the tracked features have $U/c > 1$ (fig. S2).

Westward copropagation of SSH and CHL. The revised interpretation of westward-propagating SSH as nonlinear eddies mandates a reassessment of past conclusions that the westward copropagation of CHL and SSH is indicative of Rossby wave influence on CHL. The alternative hypothesis that CHL variability is eddy-induced is examined here from 10 years of concurrent measurements of SSH and CHL in the southeastern Pacific (SEP) near 20°S that has been a focus of past studies (*6*, *7*).

The trajectories of mesoscale eddies (*18*) in the SEP are shown in Fig. 1A. Compared with eddies observed globally in the latitude range 15° to 25°, their mean amplitude is smaller (3.2 cm versus 6.2 cm) but their mean radius is the same (110 km). Because U is approximately proportional to eddy amplitude, eddies in the SEP are less nonlinear (fig. S2); 87% have $U/c > 1$.

The mean CHL distribution has a generally northward gradient over most of the SEP (Fig. 1B). The influence of eddies is evident from the sinuous character of the CHL field at any particular time (Fig. 1, C and D). The distortions of an otherwise smoothly varying CHL field are most apparent in regions of strong CHL gradient.

Eddy influence on the CHL field becomes clearer after filtering to remove the large-scale and seasonally varying CHL and SSH (*22*). Westward copropagation of CHL and SSH is apparent from time-longitude plots of the resulting anomaly fields (Fig. 2, A and B). The trajectories of the centroids of clockwise (CW) and counterclockwise (CCW) rotating eddies in the SEP coincide, respectively, with negative and positive extrema of westward-propagating SSH (Fig. 2A). The positive lag of maximum positive correlation in Fig. 2C indicates that the SSH extrema at the eddy centroids lag the extrema of westward-propagating CHL by ~1 month in the eastern SEP, decreasing to ~0.5 month in the west. There is a weaker negative correlation at negative lags of 1 to 1.5 months.

Eddy influence on CHL. To interpret the lagged correlations in Fig. 2C, anomaly CHL was composite averaged within eddy interiors in a translating and rotated coordinate system in which the large-scale CHL gradient vector is oriented at a polar angle of 90° (*22*). The CHL anomaly composites consist of dipoles with opposing signs and with different orientations in CW and CCW rotating eddies (Fig. 3A). As indicated by the ratio r in Fig. 3A, the dipoles are asymmetric in both cases with larger magnitudes in the left half of each composite, corresponding to the leading half of these westward-propagating eddies. The displacements from the eddy centroid are smaller for these primary poles than for the secondary poles of opposite sign in the trailing (right) halves of the eddies (see also fig. S4).

The negative extremum of SSH at the centroids of CW rotating eddies in the SEP is straddled by negative and positive poles of CHL to the west and east, respectively. The opposite occurs in CCW rotating eddies, for which the positive extremum of SSH at the centroids is straddled by positive and negative poles of CHL to the west and east, respectively. The parallel bands of positive and negative lagged correlations in Fig. 2C thus arise from a combination of west-

[1]College of Oceanic and Atmospheric Sciences, 104 COAS Administration Building, Oregon State University, Corvallis, OR 97331–5503, USA. [2]Northwest Research Associates, Post Office Box 3027, Bellevue, WA 98009, USA.

*To whom correspondence should be addressed. E-mail: chelton@coas.oregonstate.edu

ward propagation and the zonal alignments of the monopole extrema of SSH and dipole extrema of CHL.

The geographical patterns of anomalous CHL within the eddy interiors in this region of generally northward CHL gradient are indicative of horizontal advection of CHL by the rotational velocities of the eddies. For CW rotating eddies (Figs. 3A and 4A, top panels), the northward velocity in the western half of each eddy advects low CHL from south to north, resulting in anomalously low CHL in the northwest quadrant. The southward velocity in the eastern half of each such eddy advects high CHL from north to south, resulting in anomalously high CHL in the southeast quadrant. The opposite rotational sense of CCW rotating eddies (Figs. 3A and 4A, bottom panels) results in anomalously high and low CHL in the southwest and northeast quadrants, respectively.

The importance of composite averaging the CHL in a rotated coordinate system is clear from Fig. 4, A and B. The dipole patterns of anomaly CHL result from a combination of the rotational sense of the eddies and the direction of the CHL gradient. These dipoles are manifest as distortions of the total CHL field (Fig. 1, C and D).

The CHL anomaly within the trailing half of the eddy is generally weaker and noisier than within the leading half because the trailing half encounters a CHL field that has been distorted by the leading half. The noisiness of the secondary poles accounts for the somewhat weaker negative correlations in Fig. 2C, as well as their smaller composite average magnitudes compared with the primary poles (Fig. 3A).

Within an individual eddy, the structure of the dipole of anomaly CHL from eddy-driven advection varies, depending on the strength and orientation of the geographically and temporally varying gradient of CHL, the degree of eddy nonlinearity U/c, and the influence of other eddies that have recently perturbed the CHL field. Past confusion about geographical and temporal variations of the lag relationships between SSH and CHL is therefore not surprising.

Rotational advection of CHL by eddies is reproduced in numerical model simulations of random westward-propagating eddies in a tracer field with a northward gradient (*22*). The dipoles of anomalous tracer concentration for weakly nonlinear eddies (Fig. 3B) are very similar to the dipoles of observed CHL in Fig. 3A. The model reproduces the asymmetry of the magnitudes of the dipoles, as well as the smaller offset between the eddy centroid and the primary pole in the leading halves of the eddies compared with the secondary pole in the trailing halves. The higher rotational velocities within strongly nonlinear eddies result in tracer dipoles with larger magnitudes and with centers advected farther around the eddy interiors (Fig. 3C).

Composite averaging separately for the SEP eddies east and west of 108°W (figs. S3 and S5) reveals that the longitudinal variations of the couplet of positive and negative lagged correlations in Fig. 2C are attributable to longitudinal variations of the structures of the CHL dipoles. The shorter lag of maximum positive correlation in the west is due to smaller displacements between the eddy centroids and the primary poles of CHL anomaly in the leading halves of the eddies. The near-symmetry of the lags of positive and negative correlation bands in the east is consistent with the near-symmetric displacements of the dipole centers from the eddy centroids.

The geographical patterns of eddy-induced CHL anomalies in the SEP are similar to the patterns found in other regions of northward gradient of CHL. Composite averages of anomaly CHL computed globally between latitudes of 15° and 45° are shown in Fig. 3D for the tracked eddies within regions of northward CHL gradient (*22*). The telltale asymmetric dipole patterns from opposing meridional advection in opposite halves of the eddies are readily apparent.

Anomaly CHL was composite averaged for regions of generally southward CHL gradient by rotating the translating coordinate system

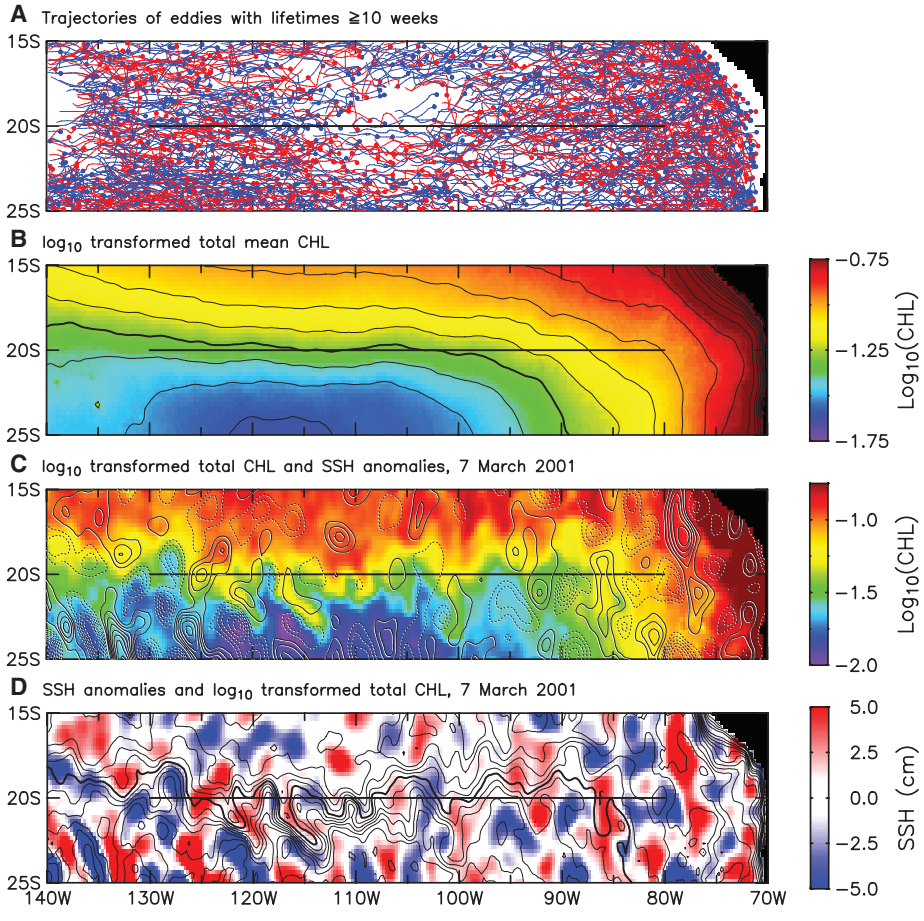

Fig. 1. Geographical characteristics of observed SSH and CHL in the SEP. (**A**) The trajectories from a 16-year data record of eddies that rotate clockwise (CW, blue lines) and counterclockwise (CCW, red lines), with the starting locations shown by solid circles. (**B**) The 10-year average $\log_{10}$(CHL) for CHL in units of mg m^{-3}, with a contour interval of $\log_{10}$(CHL) = 0.1, increasing northward, and with the thick line corresponding to $\log_{10}$(CHL) = −1.3. (**C**) An example map for 7 March 2001 showing $\log_{10}$(CHL) in color with contours of positive and negative anomaly SSH (solid and dashed lines, respectively) at intervals of 2 cm, excluding the zero contour. (**D**) The same as (C), except showing anomaly SSH in color with contours of $\log_{10}$(CHL) at the same interval as in (B). The horizontal lines in each panel are the section along which the time-longitude plots in Fig. 2 and the spectra in Fig. 5, A to C, were computed.

so that the large-scale CHL gradient vector is oriented at a polar angle of –90°. The axes of the CHL dipoles in these composite averages (Fig. 3E) are rotated ~180° relative to those in regions of northward CHL gradient. These mirrored dipoles still have larger magnitude in the leading (left) half of the westward-propagating eddies.

When $U/c > 1$, fluid is trapped within the eddy interior and transported along the eddy trajectory (*20*, *21*). This nonlinear signal of sustained transport of fluid trapped in the eddy core is not

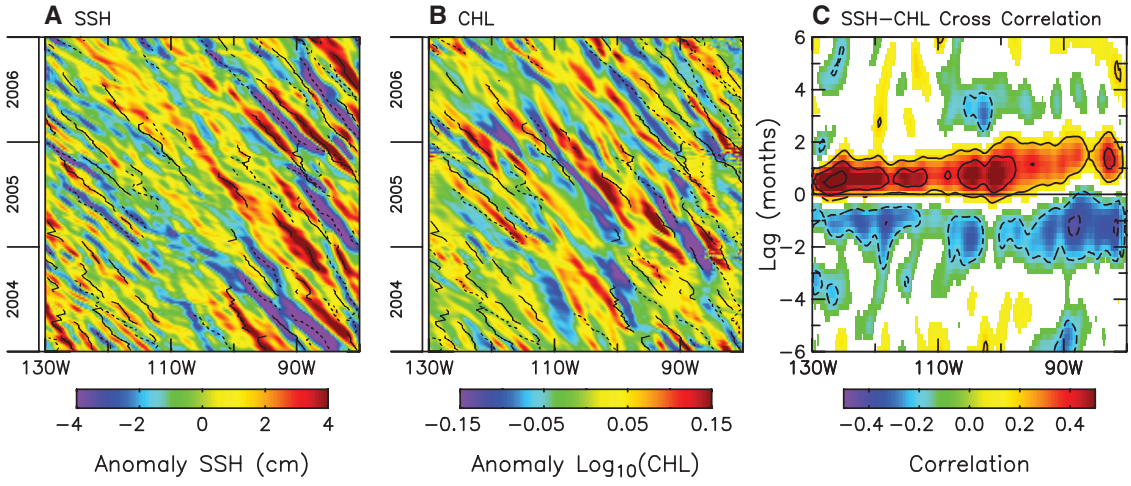

Fig. 2. Spatial and temporal variability of filtered SSH and $\log_{10}$(CHL) observations (*22*) along 20°S between 130°W and 80°W. Time-longitude sections of westward-only propagation over a 3-year portion of the 10-year period analyzed here are shown for (**A**) SSH with eddy tracks within ±2° of 20°S overlaid (dashed and solid lines for CW and CCW rotating eddies, respectively); (**B**) $\log_{10}$(CHL) with the same eddy tracks overlaid; and (**C**) the lagged cross-correlation between $\log_{10}$(CHL) at time t and SSH at time t + lag, calculated over the full 10-year data record; the white areas correspond to correlations smaller than the estimated 95% significance level of 0.083 (*22*). Positive lags correspond to $\log_{10}$(CHL) leading SSH, and the contour interval is 0.2 with the zero contour omitted for clarity. Analogous time-longitude sections and lagged cross correlations are shown for the SSH and tracer fields from a quasi-geostrophic model in fig. S6.

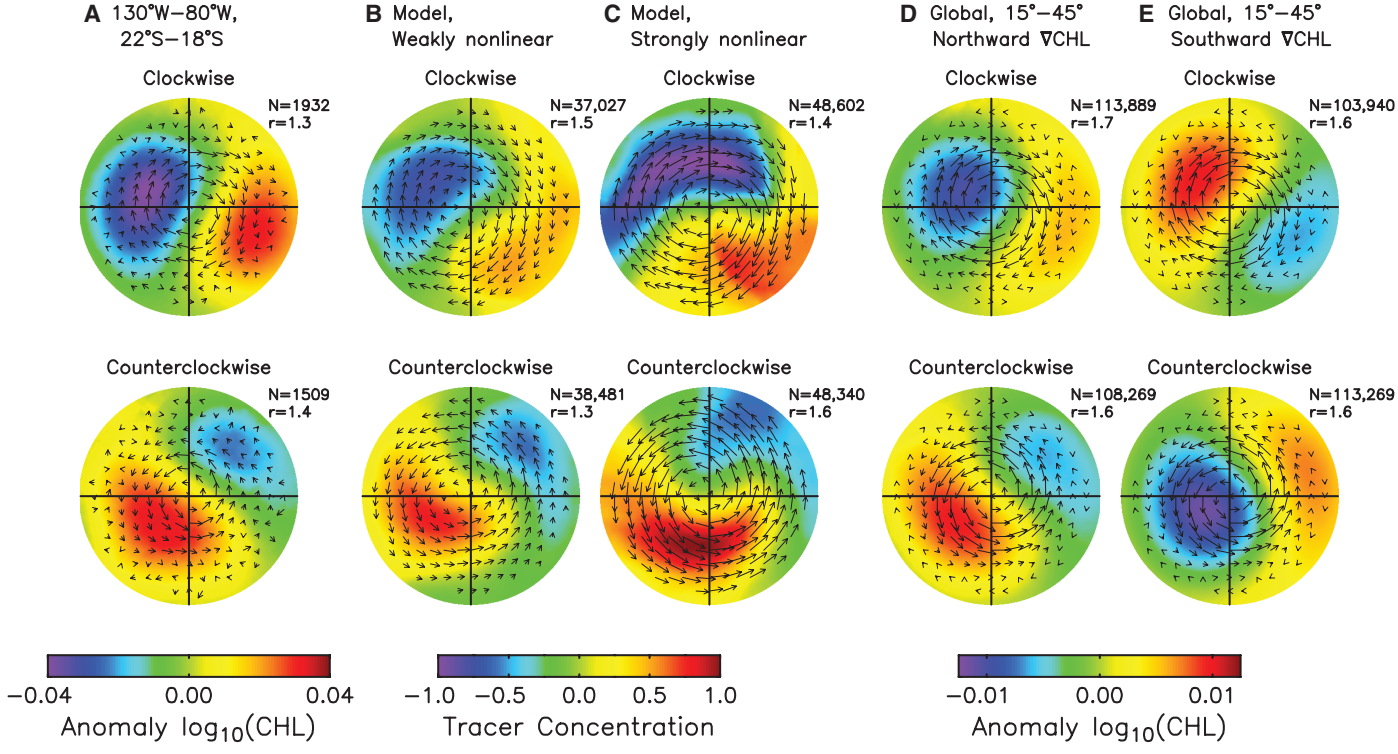

Fig. 3. Composite averages of filtered fields in a rotated and normalized coordinate system (*22*) within the interiors of CW (top panels) and CCW rotating eddies (bottom panels). (**A**) $\log_{10}$(CHL) in the region 18°S to 22°S, 130°W to 80°W. (**B**) A tracer field in a model simulation seeded with weakly nonlinear Gaussian eddies. (**C**) A tracer field in the model seeded with strongly nonlinear Gaussian eddies; (**D**) $\log_{10}$(CHL) globally between 15° and 45° latitude in regions of northward CHL gradient. (**E**) $\log_{10}$(CHL) globally between 15° and 45° latitude in regions of southward CHL gradient. The outer perimeter of each circle corresponds to twice the eddy radius scale L_s (*22*). The vectors in each panel are the gradient of the composite average SSH, which is proportional to the geostrophic velocity. The number N of eddy realizations in the composite average and the magnitude r of the ratio of the primary pole in the leading (left) half of each composite to the secondary pole in the trailing (right) half are labeled on each panel. The estimated 95% confidence intervals along profiles connecting the dipole extrema in each of these composite averages are shown in fig. S4.

the signature revealed in the CHL observations described here. The extrema of the dipole CHL features occur near the radius of maximum rotational velocity that defines the outer edge of the eddy core (*21*). As the westward-translating eddies impinge on preexisting CHL gradients, ambient fluid is advected part way around the portion of the eddy outside of the core region of closed streamlines in the translating reference frame (*20*, *21*).

Spectral analysis of SSH and CHL. Wave number–frequency spectra of SSH and CHL provide further evidence that the westward propagation of CHL is induced by nonlinear eddies. The nondispersive character of nonlinear eddies implies that the spectral variance should fall approximately along a straight line in wave number–frequency space. In contrast, the spectral variance for linear Rossby waves would be constrained to frequencies defined by their dispersion relation.

The wave number–frequency spectrum of SSH in the SEP (Fig. 5A) is clearly inconsistent with the theoretical Rossby wave dispersion relation, regardless of whether the classical theory is modified to account for effects of mean currents or rough bottom topography. Whereas the dispersion relations from these theories all flatten with increasingly negative wave number, the spectral variance of observed SSH extends to higher frequencies, straddling the

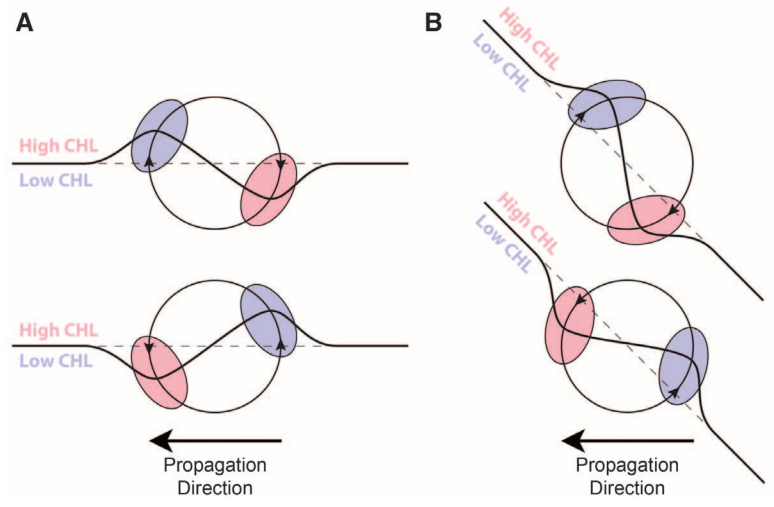

Fig. 4. Schematic diagram of eddy-driven horizontal advection of CHL for CW and CCW rotating eddies (top and bottom, respectively) propagating westward in regions where the CHL gradient is (**A**) northward and (**B**) northeastward. An otherwise smooth contour of CHL (dashed lines) is distorted by the rotational velocity field within the eddy, as shown by the solid lines. Advection of CHL within the large-scale background CHL gradient results in the positive and negative CHL anomalies shown by the red and purple regions, respectively. The dependence of the locations of these CHL anomalies on the direction of the large-scale background CHL gradient that is evident from comparison of (A) and (B) was accounted for by composite averaging in a coordinate system rotated for each eddy (*22*).

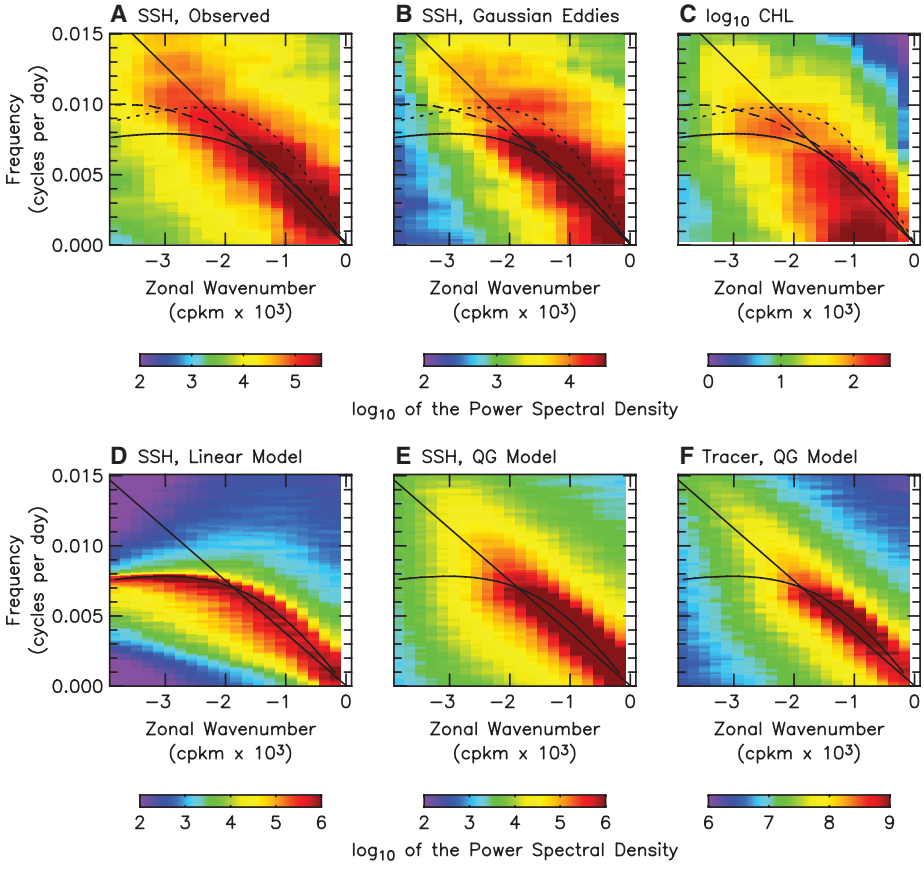

Fig. 5. Zonal (east-west) wave number–frequency spectra. (**A**) Filtered SSH for 130°W to 80°W along 20°S (see fig. S1 for SSH spectra along four other zonal sections). (**B**) SSH for Gaussian approximations of each tracked eddy for 130°W to 80°W along 20°S [different color bars are used to accommodate the smaller variance of the Gaussian approximations (*23*)]. (**C**) Filtered $\log_{10}$(CHL) for 130°W to 80°W along 20°S. (**D**) SSH from days 3000 to 15,000 of a model simulation with purely linear dynamics. (**E**) SSH from days 3000 to 15,000 of a model simulation with nonlinear quasi-geostrophic dynamics (see also fig. S7, A to C). (**F**) A tracer field in the same model simulation as in (E) (see also fig. S7, D to F). The negative wave numbers correspond to westward propagation. The units are cm for SSH, $\log_{10}$ of mg m^{-3} for CHL, and arbitrary for the tracer field. The straight lines are the mean eddy speeds from observed SSH [–4.9 cm s^{-1}, (A) to (C)] and from SSH in the model [–4.3 cm s^{-1}, (D) to (F)]. The curved lines correspond to the dispersion relations for linear Rossby waves from the classical theory for a flat bottom, no mean currents, and zero meridional (north-south) wave number (*2*) (solid), a theory that accounts for mean currents (*25*) (dashed), and a theory for rough bottom topography and no mean currents (*26*) (dotted). The latter two are irrelevant to the SSH fields from the flat-bottom model with no mean currents in (D) to (F).

straight line of constant (nondispersive) propagation speed.

We tested our hypothesis that the spectral characteristics of SSH in Fig. 5A are attributable to eddies with compact structures by constructing SSH fields consisting only of the interiors of the tracked eddies and zero outside of the eddies. Each eddy was approximated as an axisymmetric Gaussian feature with amplitude and scale estimated from the automated tracking procedure (*18*). The spectral variance of the resulting eddy-only SSH fields (Fig. 5B) straddles the same straight line as the spectrum of total SSH (*23*, *24*). The discrepancies between the wave number–frequency spectra of SSH and the Rossby wave dispersion relations are thus consistent with SSH variability being attributable to a field of propagating eddies.

The importance of nonlinearity is clarified from model simulations. The spectral variance of model SSH with linear dynamics is restricted to frequencies below the dispersion relation for Rossby waves with zero meridional wave number (Fig. 5D). The spread of variance to frequencies below this dispersion relation is from Fourier components with finite meridional wave numbers (*2*).

With nonlinear quasi-geostrophic dynamics, the spectral variance of model SSH primarily represents long-lived, coherent eddy features, in which the small-scale spectral components are phase-locked to the large-scale components (*21*). The resulting spectrum (Fig. 5E) consists of a nondispersive band along a straight line that extends to frequencies higher than are allowed by linear Rossby wave dynamics, very similar to the spectrum of observed SSH in Fig. 5A.

A short "spur" of spectral variance centered at about 0.007 cycles per day (cpd) extends along the dispersion relation in the model SSH spectrum (Fig. 5E). This spur arises from small-amplitude SSH variability outside the nonlinear cores of the eddies. The extent of the spur is found to decrease with increasing nonlinearity of the eddies (fig. S7). Although not apparent in the spectrum of observed SSH in Fig. 5A, suggestions of similar spurs exist in SSH spectra in other regions (fig. S1).

Determination of the spectrum of CHL variability is more challenging than for SSH (*22*). The spectrum of CHL in the SEP (Fig. 5C) is nonetheless similar to the spectrum of SSH. In particular, the spectral variance is concentrated along the same straight line of nondispersive variability to higher frequencies than are allowed by linear Rossby waves theories. Moreover, the spectral variance is restricted to smaller negative wave numbers than would be the case if the CHL variability were induced by linear Rossby waves. A short spur of spectral variance straddles the dispersion relation at about 0.008 cpd for the same reason discussed above for the model SSH spectra. Similar spurs are found in spectra of tracer fields in quasi-geostrophic model simulations (Fig. 5F and fig. S7, D to F). The restricted wave number extents of these spurs are an important distinction from the spectral characteristics in Fig. 5D that would be found if the CHL or tracer variability were attributable to linear Rossby waves.

Conclusions. Westward copropagation of CHL and SSH that has previously been attributed to linear Rossby waves is actually caused by nonlinear eddies that were not resolvable in the SSH fields analyzed in past studies. This eddy influence is manifest as distortions of the CHL field and is most evident in regions of strong gradients of the CHL field. Eddy influence on CHL becomes clearer after filtering. The distinctly different dipole structures of the resulting anomalous CHL distribution within the interiors of CW and CCW rotating eddies (Fig. 3, A, D, and E) and their similarity to the dipoles of a tracer field in model simulations (Fig. 3, B and C) are evidence that the dominant mechanism for eddy-induced CHL variability on the time scales >2 to 3 weeks considered here (*22*) is horizontal advection of CHL by the rotational velocity within the interior of each eddy.

The dominance of horizontal advection as the mechanism for the observed westward propagation of CHL variability has been suggested previously (*7*–*9*) but has been attributed to horizontal advection by linear Rossby waves, rather than to nonlinear eddies. [The role of eddies in defining the dipole structure of CHL anomalies has been suggested for the central North Atlantic (*14*, *15*).] The distinction between linear Rossby waves and eddies is important because the dynamics of nonlinear eddies differ fundamentally from those of linear Rossby waves. While distinct from the rotational advection identified here, eddies can trap and transport fluid parcels and their associated water properties (*20*, *21*), including nutrients, CHL, and zooplankton. They can also upwell nutrient-rich water by various mechanisms (*10*–*15*), thus stimulating the growth of phytoplankton and increasing CHL in the eddy core. Such eddy-induced enhancements often occur deep in the euphotic zone where they can be undetectable in the satellite-based measurements of near-surface ocean color (*12*–*15*).

Because of the unique trapping of fluid in the cores of nonlinear eddies, it is perhaps surprising that the CHL distribution associated with the eddies consists of dipoles with extrema outside of the eddy cores, rather than monopoles of positive or negative CHL anomalies trapped at the eddy centers. Monopole structures with very active physical-biological interaction are sometimes observed within eddy cores. In contrast to the ubiquitous presence of rotational advection around the outer portion of the eddies identified here, however, such monopole structures are usually episodic, often with time scales shorter than the 2- to 3-week filtering applied here. Although it is unclear whether the rotational advection that dominates the variability on longer time scales has important biological consequences, the results presented here clarify the dynamical importance of eddies to the observed CHL distribution.

References and Notes

1. D. B. Chelton, M. G. Schlax, *Science* **272**, 234 (1996).
2. A. E. Gill, *Atmosphere-Ocean Dynamics* (Academic Press, Cambridge, 1982).
3. P. Cipollini, D. Cromwell, P. G. Challenor, S. Raffaglio, *Geophys. Res. Lett.* **28**, 323 (2001).
4. B. M. Uz, J. A. Yoder, V. Osychny, *Nature* **409**, 597 (2001).
5. D. A. Siegel, *Nature* **409**, 576 (2001).
6. Y. Dandonneau, A. Vega, H. Loisel, Y. du Penhoat, C. Menkes, *Science* **302**, 1548 (2003).
7. P. D. Killworth, P. Cipollini, B. M. Uz, J. R. Blundell, *J. Geophys. Res.* **109**, C07002 (2004).
8. G. Charria *et al.*, *J. Mar. Res.* **64**, 43 (2006).
9. E. Gutknecht, I. Dadou, G. Charria, P. Cipollini, V. Garçon, *J. Geophys. Res.* **115**, C05004 (2010).
10. P. G. Falkowski, D. Ziemann, Z. Kolber, P. K. Bienfang, *Nature* **352**, 55 (1991).
11. D. J. McGillicuddy Jr. *et al.*, *J. Geophys. Res.* **104**, 13381 (1999).
12. D. A. Siegel, D. J. McGillicuddy Jr., E. A. Fields, *J. Geophys. Res.* **104**, 13359 (1999).
13. D. J. McGillicuddy Jr. *et al.*, *Science* **316**, 1021 (2007).
14. D. A. Siegel *et al.*, *Deep Sea Res. Part II Top. Stud. Oceanogr.* **55**, 1218 (2008).
15. D. A. Siegel, P. Peterson, D. J. McGillicuddy Jr., S. Maritorena, N. B. Nelson, *Geophys. Res. Lett.* **38**, L13608 (2011).
16. N. Ducet, P.-Y. Le Traon, G. Reverdin, *J. Geophys. Res.* **105**, 19477 (2000).
17. D. B. Chelton, M. G. Schlax, R. M. Samelson, R. A. de Szoeke, *Geophys. Res. Lett.* **34**, L15606 (2007).
18. D. B. Chelton, M. G. Schlax, R. M. Samelson, *Prog. Oceanogr.* **91**, 167 (2011).
19. J. C. McWilliams, G. R. Flierl, *J. Phys. Oceanogr.* **9**, 1155 (1979).
20. G. R. Flierl, *Geophys. Astrophys. Fluid Dyn.* **18**, 39 (1981).
21. J. J. Early, R. M. Samelson, D. B. Chelton, *J. Phys. Oceanogr.* **41**, 1535 (2011).
22. Information on methods is available as supporting online material on *Science* Online.
23. The somewhat smaller variance is due to unavoidable biases in the amplitudes of compact mesoscale features as estimated by the automated procedure (*18*).
24. The large spectral variance at small wave numbers (long wavelengths) in the spectrum of eddy-only SSH fields is easily understood qualitatively from consideration of a single Gaussian eddy. Because the Fourier transform of a Gaussian in space is a Gaussian in wave number, the associated spectrum is dominated by variance at small wave numbers. It is evident from Fig. 5B that this dominance of spectral variance at small wave numbers for a single Gaussian feature is maintained in the spectrum of a superposition of many Gaussian eddies.
25. P. D. Killworth, D. B. Chelton, R. A. de Szoeke, *J. Phys. Oceanogr.* **27**, 1946 (1997).
26. R. Tailleux, J. C. McWilliams, *J. Phys. Oceanogr.* **31**, 1461 (2001).

Acknowledgments: We thank D. McGillicuddy and T. Farrar for discussions throughout the course of this study. We also thank L.-L. Fu, V. Combes, D. Siegel, P. Cipollini, E. Shulenberger, and two anonymous reviewers for helpful comments on the manuscript. This research was supported by NASA grants NNX08AI80G and NNX08AR37G and NSF Award 0621134.

Supporting Online Material

www.sciencemag.org/cgi/content/full/science.1208897/DC1
Materials and Methods
Figs. S1 to S7
References

25 May 2011; accepted 26 August 2011
Published online 15 September 2011;
10.1126/science.1208897